

# Pion Condensation and Pion Star from Holographic QCD

Yidian Chen,<sup>1,\*</sup> Mingshan Ding,<sup>1,†</sup> Danning Li,<sup>2,‡</sup>

Kazem Bitaghsir Fadafan,<sup>3,§</sup> and Mei Huang<sup>4,¶</sup>

<sup>1</sup>*School of Physics, Hangzhou Normal University, Hangzhou, 311121, P.R. China*

<sup>2</sup>*Department of Physics and Siyuan Laboratory,  
Jinan University, Guangzhou 510632, P.R. China*

<sup>3</sup>*Faculty of Physics, Shahrood University of Technology, P.O.Box 3619995161 Shahrood, Iran*

<sup>4</sup>*School of Nuclear Science and Technology,  
University of Chinese Academy of Sciences, Beijing 100049, China*

The properties of QCD matter at finite isospin densities are investigated employing holographic hard-wall and soft-wall AdS/QCD models. It is confirmed that at high enough isospin densities, charged pions start to condense and the pion superfluid phase appears in the system. It is shown that the chiral condensate and the pion condensate can be transformed to each other and form a ‘chiral circle’ in the superfluid phase. We derived the Equation of State (EoS) for pionic matter, calculated the normalized trace anomaly  $\Delta$  and  $(\epsilon - 3p)/m_\pi^4$ , and analyzed the sound speed and adiabatic index. Additionally, we provided data on the mass-radius relation and tidal deformability of pion stars. The results indicate that the holographic models align well with lattice QCD concerning isospin density, axial-vector condensation, EoS, and trace anomaly, though discrepancies in sound speed and adiabatic index emerge at higher isospin chemical potentials. The holographic models closely match those from chiral perturbation theory ( $\chi$ PT), suggesting that they can be considered as five-dimensional description of  $\chi$ PT.

---

\* chenyardian@hznu.edu.cn

† 13149710203@163.com

‡ lidanning@jnu.edu.cn

§ bitaghsir@shahroodut.ac.ir

¶ huangmei@ucas.ac.cn

## I. INTRODUCTION

Under the condition of finite isospin chemical potential, Quantum Chromodynamics (QCD) exhibits a phenomenon: the condensation of charged pions. This phenomenon can occur in various physical environments, including heavy-ion collision experiments, the interiors of neutron stars, and the very early universe [1]. In the core of a neutron star, the excess of down quarks over up quarks generates an isospin chemical potential  $\mu_I$  [2]. Although the potential is much smaller than the baryon chemical potential  $\mu_I \ll \mu_B$ , it may explain some very heavy neutron stars [3]. Furthermore, if the early universe possessed a significant lepton flavor asymmetry, this asymmetry could be converted into a larger isospin chemical potential as the universe expanded, triggering pion condensation. This condensation could influence not only the evolution of the early universe but also leave a distinctive imprint on the spectrum of primordial gravitational waves and the mass distribution of primordial black holes [4, 5], offering valuable clues for studying the early universe.

Pion condensation in the early universe may also lead to another phenomenon: the formation of pion stars [6–8]. As one type of bosonic stars [9], pion stars are formed due to pion condensation when the pion density in space region becomes high enough, thus can gravitationally attract each other to form a self-gravitating configuration overcoming their quantum-mechanical repulsion [10]. These hypothetical stars could reveal their existence through neutrino and photon signals released during their evaporation process, or through the observation of gravitational waves in binary systems. Although the stability and lifetime of pion stars remain an open question, their lifetime is relatively short, and they could impact Big Bang nucleosynthesis, potentially affecting the primordial abundance of nuclei.

Due to the sign problem in lattice QCD [11, 12], direct calculations at finite baryon chemical potential are infeasible. Fortunately, lattice QCD calculations can be performed at finite isospin chemical potential without encountering the sign problem [13]. Significant progress has been made in lattice QCD simulations at finite isospin chemical potential, including confirming the second-order phase transition of Bose-Einstein condensation (BEC) of charged pions [14–21], studying pion dynamics, the pionic equation of state [7], and sound speed at low temperatures [22]. Beyond lattice QCD, various models like  $\chi$ PT [8, 23, 24], Nambu-Jona-Lasinio [25–31], quark-meson [32, 33], linear sigma [34, 35], random matrix

[36], and perturbative QCD [37] have been exploring QCD phase transitions and pionic matter at finite isospin chemical potential.

Inspired by the AdS/CFT correspondence principle [38–40], the bottom-up holographic QCD (HQCD) approach has become a powerful tool for studying strongly coupled gauge theories [41–52]. This method constructs an effective field theory in a higher-dimensional gravitational framework to capture the main features of QCD. Recent studies have used holographic models to explore QCD matter at finite isospin chemical potential. The properties of pionic matter have been studied in the Witten-Sakai-Sugimoto model [53, 54], also pion condensation [55–63], the QCD phase diagram [64, 65], and pion dynamics [66, 67]. The application of HQCD to neutron stars offers new insights into their extreme conditions [68–70]. These models align with astrophysical observations and have broader applications, including superconductivity [71–73]. In this paper, we extend such application to study pionic stars.

HQCD approach provides a framework to link the dynamics of an infinite number of QCD hadrons with low-energy effective theories, such as  $\chi$ PT. By integrating out heavy Kaluza-Klein modes and keeping only the lowest-lying mesons, HQCD can be reformulated into chiral effective Lagrangians [74]. This approach results in all low-energy constants of the  $\chi$ PT being expressed in terms of holographic integrals, thereby directly connecting the holographic models with chiral effective theories used in QCD. Notably, the Gell-Mann-Oakes-Renner relation, which relates the pion mass to the quark condensate and quark masses, is naturally reproduced at the lowest order of the derivative expansion in this framework [75].

The structure of this paper is as follows: Sec. II introduces the five-dimensional holographic model used in our study. Sec. III details the calculation of the pion state equation. Sec. IV presents the calculation of the sound speed and the adiabatic index. Sec. V discusses the mass-radius relation and tidal deformability of pion stars. Finally, Sec. VI summarizes and discusses our findings.

## II. MODEL SETUP

The (improved) soft-wall (SW) and hard-wall (HW) models provide a bottom-up holographic framework to explore QCD properties including hadron spectra [76–78], chiral phase transitions [79, 80], and pion condensation [55, 64, 65]. In the models, the real part of the

complex scalar field  $X$  represents sigma condensation, while its imaginary part describes the phase of the pion condensate under nonzero isospin chemical potential. These models are constructed using the probe approximation within the  $\text{AdS}_5$  or  $\text{AdS-Schwarzschild}$  black hole spacetime.

The background metric is given as

$$ds^2 = \frac{L^2}{z^2}[-f(z)dt^2 + d\vec{x}^2 + \frac{dz^2}{f(z)}], \quad (1)$$

with AdS radius  $L = 1$ , blackening factor  $f(z) = 1 - \frac{z^4}{z_h^4}$  and the horizon  $z_h$ .

The holographic QCD model with  $N_f = 2$  is constructed from  $SU(2)_L \times SU(2)_R \equiv SU(2)_V \times SU(2)_A$  flavor symmetry. The Lagrangian density can be written as

$$\mathcal{L}_5 = \text{Tr}[|D_M X|^2 + m_5^2(z)|X|^2 + \lambda|X|^4 + \frac{1}{4g_5^2}(F_{L,MN}^2 + F_{R,MN}^2)], \quad (2)$$

with the coupling  $g_5^2 = 12\pi^2/N_c = 4\pi^2$  [76]. The scalar field  $X$  and gauge fields  $A_{L/R,M}$  are dual to the quark condensate and current operators, respectively. The  $m_5$  is 5-dimensional mass and  $\lambda$  is quartic coupling. The vacuum of scalar can be given as

$$X = \frac{1}{2}(\Sigma\sigma^0 + i\Pi^a\sigma^a), \quad (3)$$

with Pauli matrices  $\sigma^a$  and identity matrix  $\sigma^0$ . Here,  $\Sigma$  and  $\Pi$  corresponds to sigma condensate  $\langle\bar{q}q\rangle$  and pion condensate  $\langle\bar{q}\gamma^5 q\rangle$ , respectively. The covariant derivative  $D_M X$  and gauge field strength  $F_{L/R}^{MN}$  are written as

$$D_M X = \partial_M X - iA_{L,M}X + iXA_{R,M}, \quad (4)$$

$$F_{L/R}^{MN} = \partial^M A_{L/R}^N - \partial^N A_{L/R}^M - i[A_{L/R}^M, A_{L/R}^N], \quad (5)$$

with  $A_{L/R,M} = A_{L/R,M}^a t^a$  and generators  $t^a$  of  $SU(2)$  group. The chiral gauge field can be redefined through vector and axial-vector fields,

$$A_{L,M} = V_M + A_M, \quad A_{R,M} = V_M - A_M, \quad (6)$$

then the covariant derivative and gauge field strength are rewritten as

$$D_M X = \partial_M X - i[V_M, X] - i\{A_M, X\}, \quad (7)$$

$$F_V^{MN} = \partial^M V^N - \partial^N V^M - i[V^M, V^N] - i[A^M, A^N], \quad (8)$$

$$F_A^{MN} = \partial^M A^N - \partial^N A^M - i[V^M, A^N] - i[A^M, V^N]. \quad (9)$$

In the following, the gauge  $A_{L/R}^z = 0$  is considered.

As discussed in Refs. [55, 64, 65], the non-vanishing condensate can be chosen as  $\Pi^{(1)} \equiv \Pi$  under  $U(1)_I$  symmetry. Moreover, the nonzero fields of model are  $A_0^{(2)} \equiv a_2$ ,  $V_0^{(3)} \equiv v$ , and  $\Sigma$ . From the holographic dictionary, the gauge fields can be expanded at the AdS boundary ( $z \rightarrow 0$ ) as

$$v \rightarrow \mu_I - C_1 n_I z^2 + \mathcal{O}(z^2), \quad a_2 \rightarrow C_2 \langle \sigma_A \rangle z^2 + \mathcal{O}(z^2), \quad (10)$$

with isospin chemical potential  $\mu_I$ , isospin density  $n_I$ , axial-vector condensate  $\langle \sigma_A \rangle$ , and normalized constants  $C_{1,2}$ . In this paper, isospin density and axial-vector condensate are obtained by (27,28), so the exact values of constants  $C_{1,2}$  are not important. For the (pseudo-)scalar fields, the expansions are

$$\Sigma \rightarrow m_q \zeta z + \frac{\langle \sigma \rangle}{\zeta} z^3 + \mathcal{O}(z^3), \quad \Pi^a \rightarrow \frac{\langle \pi^a \rangle}{\zeta} z^3 + \mathcal{O}(z^3), \quad (11)$$

with normalization constant  $\zeta$ , quark mass  $m_q$ , sigma condensate  $\langle \sigma \rangle$ , and pion condensate  $\langle \pi^a \rangle$ .

### A. Hard-Wall Model

The zero temperature is considered in the hard-wall model. So, the horizon  $z_h$  tends to infinity  $z_h \rightarrow \infty$ , and the blacken factor is  $f(z) = 1$ . The full action can be written as [55, 64]

$$S_5 = - \int d^4x \int_{\epsilon}^{z_m} dz \sqrt{-g} (\mathcal{L}_5 + \mathcal{L}_{BD}), \quad (12)$$

$$\mathcal{L}_{BD} = \text{Tr} \{ \lambda_4 z_m |X|^4 - m_2^2 z_m |X|^2 \} \delta(z - z_m), \quad (13)$$

with ultra-violet (UV) and infra-red (IR) cut-off  $\epsilon$  and  $z_m$ . The UV cut-off can be viewed as a small number that tends to zero. The Ref. [77] introduces the no-dimensional parameters  $\lambda_4$  and  $m_2$  at the boundary. The 5D mass square  $m_5^2(z)$  is viewed as a constant in the hard-wall model. According to AdS/CFT correspondence, the 5D mass is  $m_5^2 = \Delta(\Delta - 4) = -3$  with conformal dimension  $\Delta = 3$ . The values of the parameters are chosen as Refs. [55, 64]

Parameters	$m_q$ (MeV)	$\lambda$	$z_m^{-1}$ (MeV)	$\lambda_4$	$m_2^2$	$\mu_g$ (MeV)	$\mu_c$ (MeV)	$\gamma_m$	$\kappa$
HW	2.29	0	323	4.4	5.39	-	-	-	-
SW-I	3.22	80	-	-	-	440	1450	-	-
SW-II	3.58	14.7	-	-	-	440	-	3.7	1

TABLE I. The parameters of the hard-wall (HW) model and soft-wall (SW) model, taken from [55, 64, 65, 67].

and shown in Tab. I. The equations of motion are given as

$$a_2 \Pi v - \left( \frac{3}{z^2} + a_2^2 \right) \Sigma + \frac{3}{z} \Sigma' - \Sigma'' = 0, \quad (14)$$

$$v \Sigma a_2 - \left( \frac{3}{z^2} + v^2 \right) \Pi + \frac{3}{z} \Pi' - \Pi'' = 0, \quad (15)$$

$$\frac{g_5^2 \Sigma}{z^2} (v \Pi - a_2 \Sigma) - \frac{a_2'}{z} + a_2'' = 0, \quad (16)$$

$$\frac{g_5^2 \Pi}{z^2} (a_2 \Sigma - v \Pi) - \frac{v'}{z} + v'' = 0. \quad (17)$$

The following boundary conditions are considered for solving the coupled second-order differential equations. At the UV ( $z \rightarrow \epsilon$ ), the boundary conditions are

$$\left. \frac{\Sigma}{z} \right|_{\epsilon} = m_q \zeta, \quad v|_{\epsilon} = \mu_I, \quad \left. \frac{\Pi}{z} \right|_{\epsilon} = 0, \quad a_2|_{\epsilon} = 0. \quad (18)$$

with normalization constant  $\zeta = 1$ . At the IR ( $z \rightarrow z_m$ ), the boundary conditions are

$$\begin{aligned} \partial_z \Sigma|_{z_m} &= -\frac{\Sigma}{2z_m} \left( \lambda_4 (\Sigma^2 + \pi^2) - 2m_2^2 \right) \Big|_{z_m}, & \partial_z v|_{z_m} &= 0, \\ \partial_z \Pi|_{z_m} &= -\frac{\Pi}{2z_m} \left( \lambda_4 (\Sigma^2 + \pi^2) - 2m_2^2 \right) \Big|_{z_m}, & \partial_z a_2|_{z_m} &= 0. \end{aligned} \quad (19)$$

By applying UV and IR boundary conditions, combined with the Chebyshev spectral method, the equations of motion (14-17) can be solved. Furthermore, through UV expansion (11), we can obtain the condensations of sigma and pion. The condensates as a function of isospin chemical potential  $\mu_I$  are shown in Fig. 1.

## B. Soft-Wall Model

In the soft wall model, we have set the temperature values at 2 MeV, 5 MeV, 10 MeV, and 15 MeV. Numerical calculations show negligible differences in the results at different

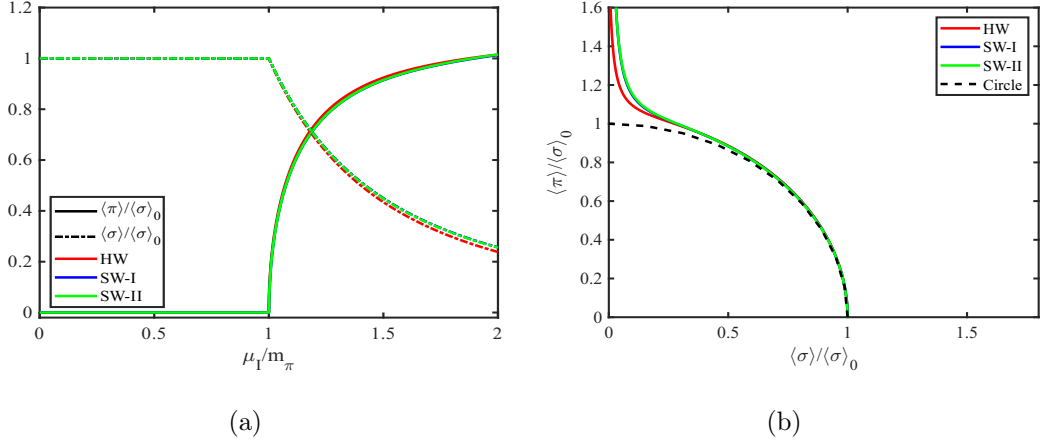


FIG. 1. Panel (a) illustrates how the sigma and pion condensates vary with the isospin chemical potential  $\mu_I$  in both the HW and SW models. Panel (b) reveals the interrelationship between the sigma and pion condensates, where the black dashed line represents the unit circle.

temperatures. Therefore, we have chosen the 10 MeV (with horizon  $z_h = 1/\pi T \simeq 31.8$   $\text{GeV}^{-1}$ ) temperature for presentation. This temperature is small compared to the pion mass  $m_\pi \simeq 140$  MeV and can be approximated as zero temperature. The full action is given as

$$S_5 = - \int d^4x \int_\epsilon^{z_h} dz \sqrt{-g} e^{-\Phi(z)} \mathcal{L}_5, \quad (20)$$

where  $\Phi(z) = \mu_g^2 z^2$  is dilaton field with constant  $\mu_g$  that match the Regge slope of light mesons. To describe the mesons spectra and chiral condensate simultaneously, we have considered two possible forms of the five-dimensional mass squared  $m_5^2(z)$  that depend on the fifth dimension, as follows:

$$m_5^2(z) = -3 - \mu_c^2 z^2, \quad (\text{SW-I}) \quad (21a)$$

$$m_5^2(z) = -3 \left( 1 + \gamma_m \tanh[\kappa \Phi(z)] \right), \quad (\text{SW-II}) \quad (21b)$$

with free parameter  $\mu_c$ ,  $\gamma_m$ , and  $\kappa$ . The leading term of them are consistent with the hard-wall model  $m_5^2 = -3$ . The values of the parameters are given from Refs. [65, 67] and shown

in Tab. I. The equations of motion of the soft-wall model are obtained as

$$\frac{\lambda \Sigma^3}{2z^2} + \frac{v \Pi a_2}{f} + \left( -\frac{a_2^2}{f} + \frac{\lambda \Pi^2 + 2m_5^2(z)}{2z^2} \right) \Sigma + \left( -f' + f \left( \frac{3}{z} + \Phi' \right) \right) \Sigma' - f \Sigma'' = 0, \quad (22)$$

$$\frac{\lambda \Pi^3}{2z^2} + \frac{v \Sigma a_2}{f} + \left( -\frac{v^2}{f} + \frac{\lambda \Sigma^2 + 2m_5^2(z)}{2z^2} \right) \Pi + \left( -f' + f \left( \frac{3}{z} + \Phi' \right) \right) \Pi' - f \Pi'' = 0, \quad (23)$$

$$\frac{g_5^2 \Sigma}{z^2} (v \Pi - a_2 \Sigma) + \left( -\frac{f}{z} - f \Phi' \right) a_2' + f a_2'' = 0, \quad (24)$$

$$\frac{g_5^2 \Pi}{z^2} (a_2 \Sigma - v \Pi) + \left( -\frac{f}{z} - f \Phi' \right) v' + f v'' = 0. \quad (25)$$

At the UV, the boundary conditions are the same as Eq. (18). At the IR ( $z \rightarrow z_h$ ), the expansions of  $\Sigma$ ,  $\Pi$ ,  $a_2$ , and  $v$  have the following form

$$\begin{aligned} \Sigma(z) &\rightarrow \Sigma_0 + \frac{6\Sigma_0 + 2z_h^2 \mu_c^2 \Sigma_0 - \lambda \Pi_0^2 \Sigma_0 - \lambda \Sigma_0^3}{8z_h} (z - z_h) + \mathcal{O}(z - z_h), \\ \Pi(z) &\rightarrow \Pi_0 + \frac{6\Pi_0 + 2z_h^2 \mu_c^2 \Pi_0 - \lambda \Sigma_0^2 \Pi_0 - \lambda \Pi_0^3}{8z_h} (z - z_h) + \mathcal{O}(z - z_h), \\ a_2(z) &\rightarrow a_{2,1}(z - z_h) + \mathcal{O}(z - z_h), \\ v(z) &\rightarrow v_1(z - z_h) + \mathcal{O}(z - z_h), \end{aligned} \quad (26)$$

with integral constants  $\Sigma_0$ ,  $\Pi_0$ ,  $a_{2,1}$ , and  $v_1$ .

Similarly, by applying boundary conditions to solve the equations of motion, we derive the condensates as a function of the isospin chemical potential  $\mu_I$ . The outcomes are presented in Fig. 1. As illustrated in Fig. 1(a), when the isospin chemical potential exceeds the mass threshold of the pion meson  $m_\pi$ , the condensates undergo significant changes. With further increases in the isospin chemical potential, sigma condensation gradually decreases, while pion condensation correspondingly increases. The combination of these two condensates  $\tilde{\sigma} = \sqrt{\sigma^2 + \pi^2}$  forms an approximate “chiral circle”, as intuitively displayed in Fig. 1(b). Both the SW and HW models predict similar condensation patterns.

It should be noted that the results obtained in this paper differ from the results in Ref. [65]. In that paper, at high enough isospin densities, the pion meson condensation tends to vanish, showing a similar effect with the baryon density effect on chiral condensate. At the same time, the shape of the formed “chiral circle” also differs. The reason for this discrepancy lies in the different approximations used in this paper compared to [65]. Specifically, in Ref. [65], the gauge field  $V$  describing the isospin current is incorporated into the background, resulting in the geometric structure of an AdS-RN black hole. In this paper, however, we follow the method of [55, 64], solving the probe action with the gauge field  $V$  included,



while keeping the background as an AdS-Schwarzschild black hole with isospin charge. Of course, one might check the validites of the two approximations by doing a full back-reaction analysis, which is out of the scope of the current work and will be left for the future.

### III. PIONIC EQUATION OF STATE

As discussed in the previous section, pion condensate emerges in the system when the non-zero isospin chemical potential reaches and exceeds the pion mass threshold. In this section, we explore the equation of state of the system with pion condensate through holographic QCD models. Based on the holographic duality principle, the partition function in gravitational theory is equivalent to quantum field theory on the boundary, that is,  $\mathcal{Z}_{\text{Gra}} = \mathcal{Z}_{\text{QCD}}$ . As a consequence of this equivalence, we can obtain the isospin density  $n_I$  and the axial vector condensate, as follows

$$n_I = \int dz \frac{\partial \mathcal{L}_5}{\partial \mu_I} = \int dz \frac{1}{z} (v \Pi^2 - a_2 \Pi \Sigma), \quad (27)$$

$$\langle \sigma \rangle_A = \int dz \frac{\partial \mathcal{L}_5}{\partial \mu_A} = \int dz \frac{1}{z} (a_2 \Sigma^2 - v \Pi \Sigma), \quad (28)$$

where we introduce the source term  $\mu_A$  for the axial vector field at the AdS boundary. During the calculation of axial-vector condensate,  $\mu_A$  is incorporated into the model, and after completing the calculation steps it is reset to 0.

The computational results of the holographic QCD model are presented in Fig. 2. The circular markers in the figure represent the lattice QCD data [7], while the solid lines correspond to the predicted results of HW, SW-I, and SW-II, respectively. The dashed lines in the figure depict the results derived from Chiral Perturbation Theory ( $\chi$ PT). At zero temperature, according to  $\chi$ PT [24], the expressions for isospin density and axial-vector condensation can be simplified to

$$n_I = f_\pi^2 \mu_I \left( 1 - \frac{m_\pi^4}{\mu_I^4} \right) \Theta(\mu_I - m_\pi), \quad (29)$$

$$\langle \sigma \rangle_A = \frac{f_\pi^2 m_\pi^2}{\mu_I} \sqrt{1 - \frac{m_\pi^4}{\mu_I^4}} \Theta(\mu_I - m_\pi), \quad (30)$$

with pion decay constant  $f_\pi$  and Heaviside step function  $\Theta$ . The different dashed lines in the figure correspond to the results obtained from the pion decay constants of different models [67, 81].

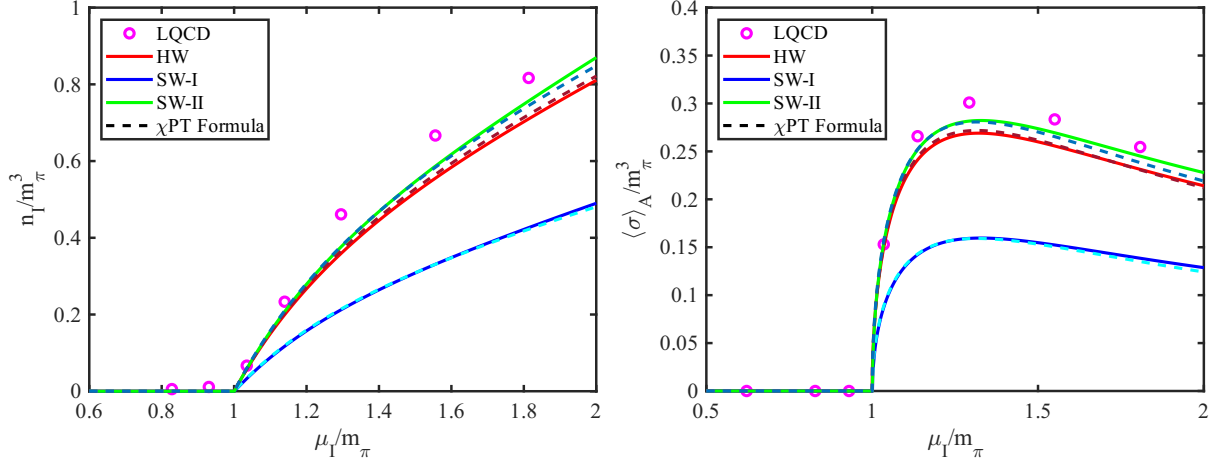


FIG. 2. The isospin density and axial vector condensate as a function of isospin chemical potential  $\mu_I$  in HW and SW model. The black dashed lines are calculations from  $\chi$ PT formulas (29) and (30).

From Fig. 2, it can be observed that the predictions of the HW model and the SW-II model match the data of the lattice QCD quite well, while the results of the SW-I model are approximately half of the lattice data. This discrepancy is because the value of the pion decay constant obtained in the SW-I model is 70.7 MeV, which is significantly lower than the results of lattice simulations. In comparison, the predicted values of the HW model and the SW-II model are closer to the experimental observation 92.4 MeV. The difference in the pion decay constants leads to a deviation between the model prediction and the data.

At zero temperature, the pionic pressure  $p$  and energy density  $\epsilon$  can be given by thermodynamic relations

$$p = \frac{\log \mathcal{Z}_{\text{QCD}}}{V} = \int_0^{\mu_I} d\mu'_I n_I(\mu'_I), \quad \epsilon = -p + \mu_I n_I. \quad (31)$$

The solid lines in Fig. 3 show the predicted results of our model, while the data from lattice QCD are presented in the circles. Additionally, the Figs. 3(b) and 3(c) display the normalized trace anomalies  $\Delta = 1/3 - p/\epsilon$  and  $(\epsilon - 3p)/m_\pi^4$ , respectively. In these sub-figures, the black dashed lines correspond to the predictions of  $\chi$ PT [22].

It can be observed from Fig. 3 that the predictions of the HW and the SW-II models are in good agreement with the lattice QCD data [7], whereas the results of the SW-I model are significantly different from the data, which is mainly due to the difference in the isospin density. For the equation of state, the holographic QCD models' predictions show

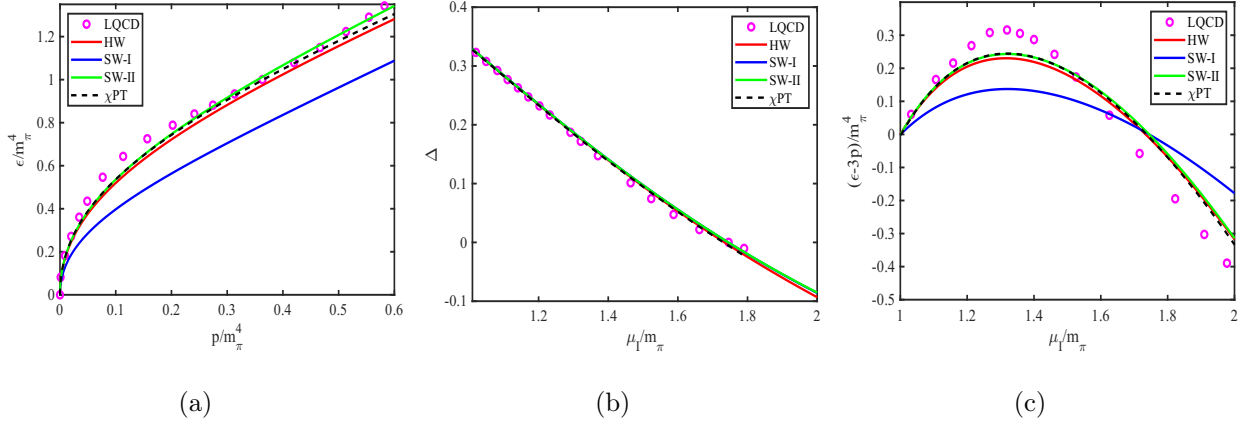


FIG. 3. The equation of state, normalized trace anomalies  $\Delta = 1/3 - p/\epsilon$  and  $(\epsilon - 3p)/m_\pi^4$  in HW and SW model. The magenta circles represent lattice QCD data [7]. The black dashed lines are calculations from  $\chi$ PT [22].

an approximately linear growth trend at high isospin chemical potential, while the lattice QCD data exhibit different growth characteristics. This discrepancy may arise from the fact that we neglected the contribution of the gravitational background in our calculations and only considered the probe approximation.

For the trace anomaly  $\Delta$ , the results of the holographic models are similar to the results of  $\chi$ PT, both showing a linearly decreasing trend. However, the lattice QCD data show a change in slope when the isospin chemical potential is around  $1.7 m_\pi$ . For the trace anomaly  $(\epsilon - 3p)/m_\pi^4$ , the predictions of models are closer to the results of the  $\chi$ PT. However, at the isospin chemical potential of about  $1.3 m_\pi$ , neither of the models can reach the maximum value shown by the lattice data.

#### IV. THE SPEED OF SOUND

From the equation of state derived in the previous section, we are able to calculate two quantities for astrophysical observations: the speed of sound  $c_s$  and the adiabatic index  $\gamma$ . The square of the speed of sound is defined as

$$c_s^2 = \frac{\partial p}{\partial \epsilon}, \quad (32)$$

and the adiabatic index is given as

$$\gamma = \frac{d \log p}{d \log \epsilon} = \frac{\epsilon}{p} c_s^2. \quad (33)$$

Fig. 4 illustrates the results of the speed of sound and the adiabatic index for the isospin chemistry potential and compares them with the lattice QCD data and the  $\chi$ PT calculations. The results indicate that the predictions of the holographic model are very close to the  $\chi$ PT calculations, and at low chemical potentials, the holographic model agrees well with the lattice data. However, when the isospin chemical potential exceeds  $1.2 m_\pi$ , significant differences begin to emerge between the holographic model and lattice data. Specifically, when the chemical potential reaches  $1.5 m_\pi$ , lattice data show that the speed of sound reaches a maximum and then decreases with increasing chemical potential, exhibiting non-monotonic behavior, while the holographic model predicts a continuous increase in the speed of sound. It is worth noting that at two specific  $\mu_I$ , the normalized trace anomaly is zero, the corresponding sound velocity square is 0 and 0.65, both are not equal to  $1/3$ . It needs more investigation whether conformality should be measured by the vanishing trace anomaly [82] or  $c_s^2 = 1/3$ .

In the conformal limit, the adiabatic index should approach  $\gamma = 1$ , but spontaneous chiral symmetry breaking can cause it to increase to about  $\gamma \simeq 2$ , which is discussed in detail in Ref. [83]. The adiabatic index value of 1.75 is considered the quark matter bound for distinguishing between two core matter states of neutron stars. The predictions of the holographic model show that the adiabatic index reaches a peak at an isospin chemical potential of about  $1.25 m_\pi$ , then gradually decreases to approach 2, suggesting that the system may always be near the chiral symmetry broken phase. In contrast, lattice QCD data show an extreme value of the adiabatic index at an isospin chemical potential of about  $1.4 m_\pi$ , approximately 2.4, and then it drops to 1.3, indicating that the system may have undergone a crossover from BEC to BCS. This difference may be due to the fact that the holographic models do not take into account the contribution of the gluon background in the calculations. If gravitational background were included in the model, similar phase transition behavior might be observed. Furthermore, as mentioned above, within the approximation used in Ref. [65], at high isospin density, both the chiral condensate and pion condensate will vanish, which in some sense turns the system from a tightly combined BEC status (meson degree of freedom) to a loosely correlated BCS status (quark degree of freedom). Therefore, similar behavior of crossover from BEC to BCS might appear in that scenario, and in the full back-reaction study as well. However, in this work, we will stick to the current scenario and leave the full back-reaction analysis to the future.

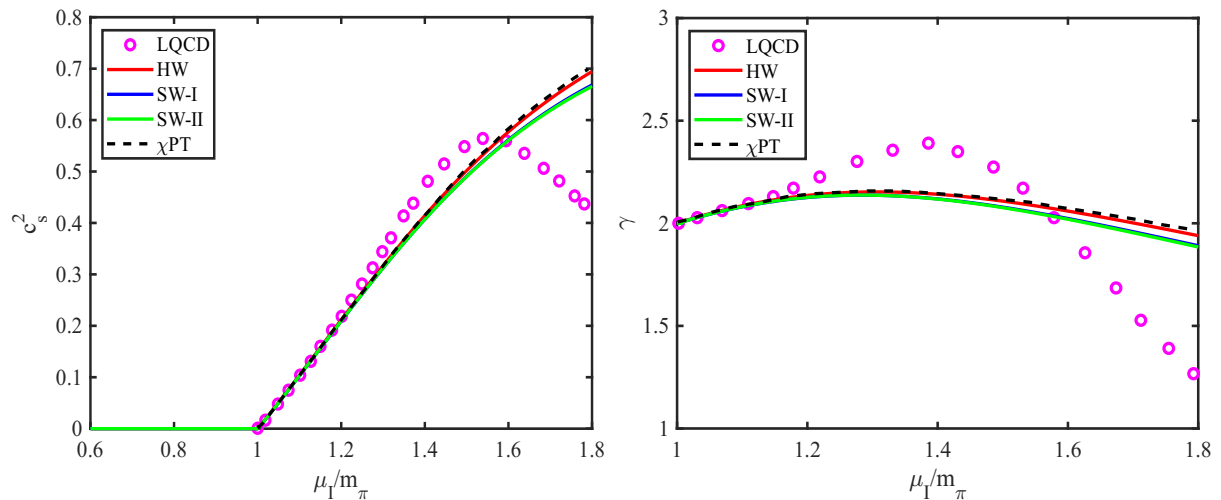


FIG. 4. The speed of sound and the adiabatic index as a function of the isospin chemical potential in the HW and SW models. The black dashed lines are calculations from  $\chi$ PT and the magenta circles are the lattice QCD data from Ref. [22].

Overall, the HW and SW models provide us with profound insights into strongly coupled pionic matter, but the comparison with lattice QCD data also reveals the limitations of these models. Future research can focus on more precise model parameterization or the development of gravitational frameworks to more comprehensively describe these complex phenomena.

The results from Sec. III and IV indicate that both the holographic soft-wall and hard-wall models yield results similar to those of  $\chi$ PT. In particular, the speed of sound and the adiabatic index from these models align closely and show a consistent discrepancy with lattice data. This suggests a potential equivalence between holographic models and  $\chi$ PT. As noted in Ref. [75], integrating out the heavy Kaluza-Klein modes results in a four-dimensional chiral effective action. A similar discussion is found in Ref. [62], where the holographic model is used to derive and reproduce the formula (29) of  $\chi$ PT. These findings imply that holographic models share a common ground with  $\chi$ PT in capturing the physics of strong interactions.

## V. PION STARS

In the previous discussion, we studied the pionic equation of state and observed its consistency with lattice QCD data, as well as similar behavior to the results of  $\chi$ PT. This section will further explore the physical properties of pion stars based on the equation of state.

In the very early universe, asymmetry in lepton flavors led to the phenomenon of pion condensation, which eventually resulted in the formation of pion stars. Pion stars are a type of Bose stars [9, 84, 85], notable for their existence without the need for new physics beyond the Standard Model. These celestial bodies maintain electrical neutrality and beta equilibrium through the presence of electrons, muons, and their neutrinos. According to Ref. [86], leptons make a significant contribution to the star's equation of state. However, in this discussion, we will temporarily disregard the impact of leptons on the overall equation of state and focus on other characteristics of pion stars.

### A. Mass-radius relation

The Tolman-Oppenheimer-Volkoff (TOV) equations originate from general relativity, describing the hydrostatic equilibrium state under the assumption of spherical symmetry. Combined with the equation of state, we can calculate the mass  $M$  and radius  $R$  of pion stars. The form of the TOV equations are as follow,

$$\frac{d}{dr}p(r) + [p(r) + \epsilon(r)] \frac{G[m(r) + 4\pi r^3 P(r)]}{r^2 \left[1 - 2\frac{Gm(r)}{r}\right]} = 0, \quad (34)$$

$$\frac{d}{dr}m(r) - 4\pi r^2 \epsilon(r) = 0, \quad (35)$$

with radial coordinate  $r$  and 4D Newtonian gravitational constant  $G$ . The pressure  $p$  and the energy density  $\epsilon$  both depend on the radial coordinate. Furthermore,  $m(r)$  represents the gravitational mass within the radius  $r$ . The solution of the equations employed the following boundary conditions:

$$m(r=0) = 0, \quad p(r=r_B) = 0, \quad (36)$$

with the radius of the star  $r_B = R$ . The total mass of the pion star is  $M = m(r_B)$ .

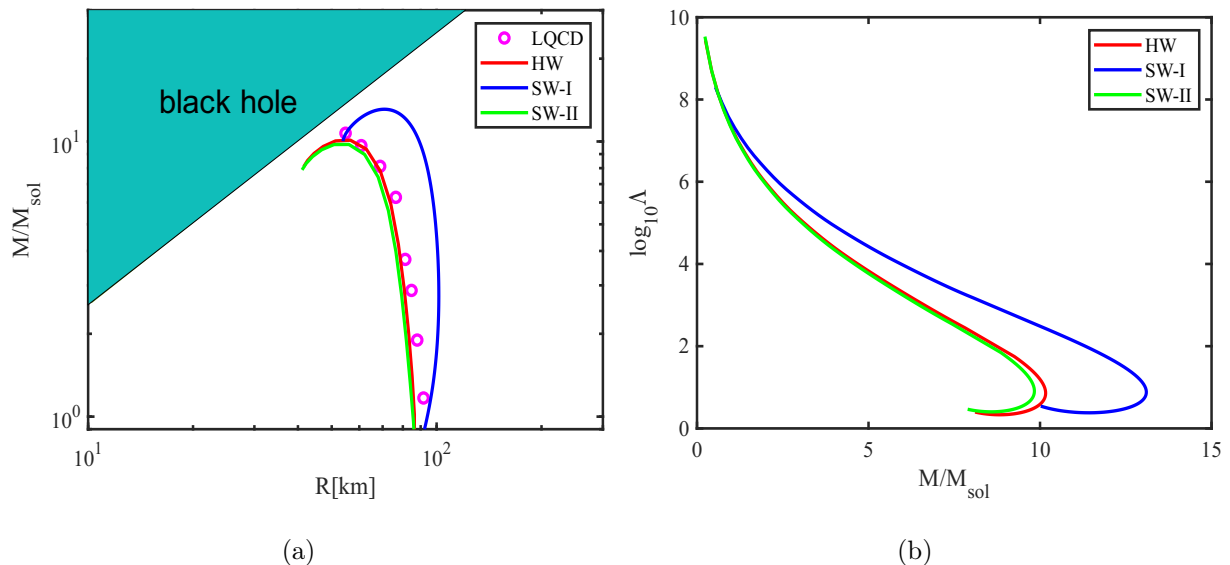


FIG. 5. The mass-radius relation and tidal deformability of pion stars. The magenta circles are the mass-radius relation obtained through the equation of state from lattice QCD data Ref. [22].

Using the pionic equation of state obtained in the previous section, we derived the mass-radius relation for pion stars, as shown in Fig. 5(a). The solid lines of different colors in the figure represent the results of the HW and SW models, while the magenta circles are the mass-radius relations obtained through the equation of state from lattice data. It can be seen from the figure that, due to the proximity of the equation of state to the lattice data, the HW and SW-II models are similar to the lattice results, while the SW-I model predicts a larger upper limit of mass. Overall, the estimated radius of pion stars is between 50-100 kilometers, with the maximum mass reaching 10 times the mass of the sun, which is significantly different from the neutron stars with a radius of 10 kilometers and a maximum mass of 2 times the mass of the sun. If electrons and muons, as well as  $\beta$  equilibrium, are further considered, different mass-radius relations for pion stars will be obtained, as detailed in Ref. [7].

## B. Tidal deformability

Finally, we investigated the dimensionless tidal deformability  $\Lambda$ ,

$$\Lambda = \frac{2k_2}{3C^5}, \quad (37)$$

where

$$\begin{aligned}
k_2 = & \frac{8C^5}{5}(1-2C)^2[2+2C(y-1)-y]\{2C[6-3y+3C(5y-8)] \\
& + 4C^3[13-11y+C(3y-2)+2C^2(1+y)] \\
& + 3(1-2C)^2[2-y+2C(y-1)]\ln(1-2C)\}^{-1},
\end{aligned} \tag{38}$$

and

$$C = \frac{GM}{r_B}, \quad y = \frac{r_B\beta(r_B)}{H(r_B)}. \tag{39}$$

The functions  $H(r)$  and  $\beta(r)$  satisfy following equations,

$$\begin{aligned}
\frac{d}{dr}\beta(r) - \frac{2H(r)}{\left[1-2\frac{Gm(r)}{r}\right]} & \left\{ -2\pi G \left[ 5\epsilon(r) + 9P(r) + \frac{\frac{d}{dr}\epsilon(r)}{\frac{d}{dr}P(r)}[P(r) + \epsilon(r)] \right] \right. \\
& + \frac{3}{r^2} + \frac{2}{1-2\frac{Gm(r)}{r}} G^2 \left[ \frac{M}{r^2} + 4\pi r P(r) \right]^2 \Big\} \\
& - \frac{2\beta(r)}{r \left[ 1 - 2\frac{Gm(r)}{r} \right]} \left\{ -1 + \frac{Gm(r)}{r} + 2\pi G r^2 [\epsilon(r) - P(r)] \right\} = 0,
\end{aligned} \tag{40}$$

and

$$\beta(r) - \frac{d}{dr}H(r) = 0, \tag{41}$$

with the boundary conditions

$$H(r \rightarrow 0) \rightarrow a_0 r^2, \quad \beta(r \rightarrow 0) \rightarrow 2a_0 r. \tag{42}$$

The choice of the constant  $a_0$  has no effect on the final result.

The numerical results are shown in Fig. 5(b). It can be seen from the figure that for a mass of 5 solar masses, the tidal deformability is approximately  $10^4$ .

## VI. CONCLUSION AND DISCUSSION

This study uses holographic hard-wall and soft-wall models to explore the relation between pion condensation, isospin density, axial-vector condensation, and isospin chemical potential. We successfully derived the EoS for pionic matter using thermodynamic relations. Additionally, we calculated the normalized trace anomaly  $\Delta$  and  $(\epsilon - 3p)/m_\pi^4$ . Using the



EoS, we analyzed the sound speed and adiabatic index, which are crucial for understanding the physical characteristics of pion stars. We also obtained the mass-radius relation and tidal deformability of pion stars, providing quantitative results for studying these bosonic stars.

The results from the holographic models show good agreement with lattice QCD in terms of isospin density, axial-vector condensation, EoS, and normalized trace anomaly. This indicates that holographic models are highly reliable in describing the QCD phase diagram. However, discrepancies were found in the calculations of the sound speed and adiabatic index. At low isospin chemical potentials, the results of the holographic models and lattice QCD coincide. Still, when the isospin chemical potential exceeds  $1.5 m_\pi$ , the sound speed in lattice data reaches a maximum and then starts to decrease, while it continues to rise in the holographic model. Similarly, when the isospin chemical potential exceeds  $1.4 m_\pi$ , the adiabatic index in lattice QCD reaches a maximum and then rapidly decreases, while it remains around 2 in the holographic model. These differences might indicate a crossover from BEC to BCS at high isospin chemical potentials, which the holographic model fails to capture.

Further analysis shows that the results from the holographic models are very similar to those from  $\chi$ PT. In the calculations of isospin density and axial-vector condensation, the results of the holographic models are highly consistent with the approximate formulas of  $\chi$ PT. In addition, the calculations of the trace anomaly, sound speed, and adiabatic index also align with the predictions of  $\chi$ PT. Notably, the approximate linear decrease in the trace anomaly, the continuous increase in sound speed with isospin chemical potential, and the adiabatic index remaining around 2 are all consistent with  $\chi$ PT calculations. This suggests that the holographic model can be considered a five-dimensional  $\chi$ PT to some extent, offering a new perspective for studying AdS/QCD.

In this study, we employed the holographic approach to the pionic equation of state to calculate the mass-radius relation and tidal deformability of pion stars. Our calculations revealed that the typical radius of a pion star is approximately 100 kilometers, with a mass around  $10 M_\odot$ . The tidal deformability,  $\Lambda$ , ranges from 10 to  $10^8$ . The presence of lepton flavor asymmetry in the early universe [4, 5] could potentially drive the formation of pion condensation. Additionally, when the energy density in regions of high isospin density reaches a critical threshold, gravitational collapse may occur, leading to the formation of

pion stars. However, in this paper, we have not fully explored the formation mechanism or lifetime of pion stars, which are topics that require further investigation.

Our approach differs slightly from the scheme in Ref. [65], leading to qualitative differences in the results. Further research is needed to clarify the reasons for these differences and their impact on physical phenomena. The current study neglects the contribution of gluon dynamics, which may be one of the reasons for the inconsistencies between the holographic model and lattice QCD data. Future studies could consider coupling the gravitational background with the system to reproduce lattice QCD results, thereby gaining a more comprehensive understanding of the  $T - \mu_I$  phase diagram and properties of strongly interacting pionic matter.

### ACKNOWLEDGMENTS

This work is supported by the National Natural Science Foundation of China (NSFC) Grant Nos: 12305136, 12275108, 12235016, 12221005, the start-up funding of Hangzhou Normal University under Grant No. 4245C50223204075, and the Strategic Priority Research Program of Chinese Academy of Sciences under Grant No XDB34030000, and the Fundamental Research Funds for the Central Universities.

- 
- [1] Dominik J. Schwarz and Maik Stuke. Lepton asymmetry and the cosmic QCD transition. *JCAP*, 11:025, 2009. [Erratum: *JCAP* 10, E01 (2010)].
  - [2] Arkady B. Migdal, E. E. Saperstein, M. A. Troitsky, and D. N. Voskresensky. Pion degrees of freedom in nuclear matter. *Phys. Rept.*, 192:179–437, 1990.
  - [3] James M. Lattimer and Maddapa Prakash. Neutron Star Observations: Prognosis for Equation of State Constraints. *Phys. Rept.*, 442:109–165, 2007.
  - [4] Steven L. Liebling and Carlos Palenzuela. Dynamical boson stars. *Living Rev. Rel.*, 26(1):1, 2023.
  - [5] Volodymyr Vovchenko, Bastian B. Brandt, Francesca Cuteri, Gergely Endrődi, Fazlollah Hajkarim, and Jürgen Schaffner-Bielich. Pion condensation in the early universe at nonvanishing lepton flavor asymmetry and its gravitational wave signatures. *Physical Review*

- Letters*, 126(1):012701, 2021.
- [6] Yu. L. Vartanyan, G. S. Adzhyan, and G. B. Alaverdyan. Pion stars. *Sov. Astron.*, 28:396–401, 1984.
  - [7] Bastian B. Brandt, Gergely Endrodi, Eduardo S. Fraga, Mauricio Hippert, Jurgen Schaffner-Bielich, and Sebastian Schmalzbauer. New class of compact stars: Pion stars. *Physical Review D: Particles and Fields*, 98(9):094510, 2018.
  - [8] Stefano Carignano, Luca Lepori, Andrea Mammarella, Massimo Mannarelli, and Giulia Pagliaroli. Scrutinizing the pion condensed phase. *Eur. Phys. J. A*, 53(2):35, 2017.
  - [9] Philippe Jetzer. Boson stars. *Phys. Rept.*, 220:163–227, 1992.
  - [10] Burkhard Kleihaus, Jutta Kunz, Claus Lammerzahl, and Meike List. Charged Boson Stars and Black Holes. *Phys. Lett. B*, 675:102–115, 2009.
  - [11] Ian Barbour, Nasr-Eddine Behilil, Elbio Dagotto, Frithjof Karsch, Adriana Moreo, Michael Stone, and H. W. Wyld. Problems with Finite Density Simulations of Lattice QCD. *Nucl. Phys. B*, 275:296–318, 1986.
  - [12] J. B. Kogut, M. P. Lombardo, and D. K. Sinclair. Quenched QCD at finite density. *Phys. Rev. D*, 51:1282–1291, 1995.
  - [13] J. B. Kogut and D. K. Sinclair. Quenched lattice QCD at finite isospin density and related theories. *Phys. Rev. D*, 66:014508, 2002.
  - [14] J. B. Kogut and D. K. Sinclair. Lattice QCD at finite isospin density at zero and finite temperature. *Physical Review D: Particles and Fields*, 66(ANL-HEP-PR-02-016):034505, 2002.
  - [15] J. B. Kogut and D. K. Sinclair. The Finite temperature transition for 2-flavor lattice QCD at finite isospin density. *Phys. Rev. D*, 70:094501, 2004.
  - [16] Philippe de Forcrand, Mikhail A. Stephanov, and Urs Wenger. On the phase diagram of QCD at finite isospin density. *PoS, LATTICE2007*:237, 2007.
  - [17] Paolo Cea, Leonardo Cosmai, Massimo D’Elia, Alessandro Papa, and Francesco Sanfilippo. The critical line of two-flavor QCD at finite isospin or baryon densities from imaginary chemical potentials. *Phys. Rev. D*, 85:094512, 2012.
  - [18] William Detmold, Kostas Orginos, and Zhifeng Shi. Lattice QCD at non-zero isospin chemical potential. *Phys. Rev. D*, 86:054507, 2012.
  - [19] G. Endrödi. Magnetic structure of isospin-asymmetric QCD matter in neutron stars. *Phys. Rev. D*, 90(9):094501, 2014.

- [20] B. B. Brandt, G. Endrodi, and S. Schmalzbauer. QCD phase diagram for nonzero isospin-asymmetry. *Phys. Rev. D*, 97(5):054514, 2018.
- [21] Bastian B. Brandt and Gergely Endrodi. Reliability of Taylor expansions in QCD. *Phys. Rev. D*, 99(1):014518, 2019.
- [22] Bastian B. Brandt, Francesca Cuteri, and Gergely Endrodi. Equation of state and speed of sound of isospin-asymmetric QCD on the lattice. *JHEP*, 07:055, 2023.
- [23] D. B. Kaplan and A. E. Nelson. Strange Goings on in Dense Nucleonic Matter. *Phys. Lett. B*, 175:57–63, 1986.
- [24] D. T. Son and Misha A. Stephanov. QCD at finite isospin density. *Physical Review Letters*, 86:592–595, 2001.
- [25] D. Toublan and J. B. Kogut. Isospin chemical potential and the QCD phase diagram at nonzero temperature and baryon chemical potential. *Phys. Lett. B*, 564:212–216, 2003.
- [26] A. Barducci, R. Casalbuoni, Giulio Pettini, and L. Ravagli. A Calculation of the QCD phase diagram at finite temperature, and baryon and isospin chemical potentials. *Phys. Rev. D*, 69:096004, 2004.
- [27] Lian-yi He, Meng Jin, and Peng-fei Zhuang. Pion superfluidity and meson properties at finite isospin density. *Phys. Rev. D*, 71:116001, 2005.
- [28] Gao-feng Sun, Lianyi He, and Pengfei Zhuang. BEC-BCS crossover in the Nambu-Jona-Lasinio model of QCD. *Phys. Rev. D*, 75:096004, 2007.
- [29] Tao Xia, Lianyi He, and Pengfei Zhuang. Three-flavor Nambu–Jona-Lasinio model at finite isospin chemical potential. *Phys. Rev. D*, 88(5):056013, 2013.
- [30] Jingyi Chao, Mei Huang, and Andrey Radzhabov. Charged pion condensation in anti-parallel electromagnetic fields and nonzero isospin density. *Chin. Phys. C*, 44(3):034105, 2020.
- [31] Hui Zhang, Defu Hou, and Jinfeng Liao. Mesonic Condensation in Isospin Matter under Rotation. *Chin. Phys. C*, 44(11):111001, 2020.
- [32] Prabal Adhikari, Jens O. Andersen, and Patrick Kneschke. Pion condensation and phase diagram in the Polyakov-loop quark-meson model. *Phys. Rev. D*, 98(7):074016, 2018.
- [33] Ziyue Wang and Pengfei Zhuang. Meson spectral functions at finite temperature and isospin density with the functional renormalization group. *Phys. Rev. D*, 96(1):014006, 2017.
- [34] Marcelo Loewe, Cristian Villavicencio, and R. Zamora. Linear sigma model and the formation of a charged pion condensate in the presence of an external magnetic field. *Phys. Rev. D*,

- 89(1):016004, 2014.
- [35] Ziyue Wang and Pengfei Zhuang. Critical Behavior and Dimension Crossover of Pion Superfluidity. *Phys. Rev. D*, 94(5):056012, 2016.
  - [36] B. Klein, D. Toublan, and J. J. M. Verbaarschot. The QCD phase diagram at nonzero temperature, baryon and isospin chemical potentials in random matrix theory. *Phys. Rev. D*, 68:014009, 2003.
  - [37] Thorben Graf, Juergen Schaffner-Bielich, and Eduardo S. Fraga. Perturbative thermodynamics at nonzero isospin density for cold QCD. *Phys. Rev. D*, 93(8):085030, 2016.
  - [38] Juan Martin Maldacena. The Large N limit of superconformal field theories and supergravity. *Adv. Theor. Math. Phys.*, 2:231–252, 1998.
  - [39] S. S. Gubser, Igor R. Klebanov, and Alexander M. Polyakov. Gauge theory correlators from noncritical string theory. *Phys. Lett. B*, 428:105–114, 1998.
  - [40] Edward Witten. Anti-de Sitter space and holography. *Adv. Theor. Math. Phys.*, 2:253–291, 1998.
  - [41] U. Gursoy and E. Kiritsis. Exploring improved holographic theories for QCD: Part I. *JHEP*, 02:032, 2008.
  - [42] U. Gursoy, E. Kiritsis, and F. Nitti. Exploring improved holographic theories for QCD: Part II. *JHEP*, 02:019, 2008.
  - [43] Steven S. Gubser and Abhinav Nellore. Mimicking the QCD equation of state with a dual black hole. *Phys. Rev. D*, 78:086007, 2008.
  - [44] Steven S. Gubser, Abhinav Nellore, Silviu S. Pufu, and Fabio D. Rocha. Thermodynamics and bulk viscosity of approximate black hole duals to finite temperature quantum chromodynamics. *Phys. Rev. Lett.*, 101:131601, 2008.
  - [45] Oliver DeWolfe, Steven S. Gubser, and Christopher Rosen. A holographic critical point. *Phys. Rev. D*, 83:086005, 2011.
  - [46] Danning Li and Mei Huang. Dynamical holographic QCD model for glueball and light meson spectra. *JHEP*, 11:088, 2013.
  - [47] Danning Li, Jinfeng Liao, and Mei Huang. Enhancement of jet quenching around phase transition: Result from the dynamical holographic model. *Physical Review D: Particles and Fields*, 89(12):126006, 2014.
  - [48] Danning Li, Song He, and Mei Huang. Temperature dependent transport coefficients in a

- dynamical holographic QCD model. *JHEP*, 06:046, 2015.
- [49] Kazem Bitaghsir Fadafan, Farideh Kazemian, and Andreas Schmitt. Towards a holographic quark-hadron continuity. *JHEP*, 03:183, 2019.
  - [50] Xun Chen, Danning Li, Defu Hou, and Mei Huang. Quarkyonic phase from quenched dynamical holographic QCD model. *JHEP*, 03:073, 2020.
  - [51] Yidian Chen, Danning Li, and Mei Huang. The dynamical holographic QCD method for hadron physics and QCD matter. *Commun. Theor. Phys.*, 74(9):097201, 2022.
  - [52] Rong-Gen Cai, Song He, Li Li, and Yuan-Xu Wang. Probing QCD critical point and induced gravitational wave by black hole physics. *Physical Review D: Particles and Fields*, 106(12):L121902, 2022.
  - [53] Nicolas Kovensky, Aaron Poole, and Andreas Schmitt. Phases of cold holographic QCD: Baryons, pions and rho mesons. *SciPost Phys.*, 15(4):162, 2023.
  - [54] Nicolas Kovensky and Andreas Schmitt. Thermal pion condensation: holography meets lattice QCD. 7 2024.
  - [55] Hiroki Nishihara and Masayasu Harada. Equation of state in the pion condensation phase in asymmetric nuclear matter using a holographic QCD model. *Physical Review D: Particles and Fields*, 90(11):115027, 2014.
  - [56] Youngman Kim, Chang-Hwan Lee, and Ho-Ung Yee. Holographic Nuclear Matter in AdS/QCD. *Phys. Rev. D*, 77:085030, 2008.
  - [57] Andrei Parnachev. Holographic QCD with Isospin Chemical Potential. *JHEP*, 02:062, 2008.
  - [58] Ofer Aharony, Kasper Peeters, Jacob Sonnenschein, and Marija Zamaklar. Rho meson condensation at finite isospin chemical potential in a holographic model for QCD. *JHEP*, 02:071, 2008.
  - [59] Pallab Basu, Jianyang He, Anindya Mukherjee, and Hsien-Hang Shieh. Superconductivity from D3/D7: Holographic Pion Superfluid. *JHEP*, 11:070, 2009.
  - [60] Martin Ammon, Johanna Erdmenger, Matthias Kaminski, and Patrick Kerner. Flavor Superconductivity from Gauge/Gravity Duality. *JHEP*, 10:067, 2009.
  - [61] Bum-Hoon Lee, Shahin Mamedov, Siyoung Nam, and Chanyong Park. Holographic meson mass splitting in the Nuclear Matter. *JHEP*, 08:045, 2013.
  - [62] Dylan Albrecht and Joshua Erlich. Pion condensation in holographic QCD. *Phys. Rev. D*, 82:095002, 2010.

- [63] Meng Lv, Danning Li, and Song He. Pion condensation in a soft-wall AdS/QCD model. *JHEP*, 11:026, 2019.
- [64] Hiroki Nishihara and Masayasu Harada. Enhancement of Chiral Symmetry Breaking from the Pion condensation at finite isospin chemical potential in a holographic QCD model. *Physical Review D: Particles and Fields*, 89(7):076001, 2014.
- [65] Xuanmin Cao, Hui Liu, Danning Li, and Guanning Ou. QCD phase diagram at finite isospin chemical potential and temperature in an IR-improved soft-wall AdS/QCD model. *Chinese Physics C*, 44(8):083106, 2020.
- [66] Xuanmin Cao, Matteo Baggioli, Hui Liu, and Danning Li. Pion dynamics in a soft-wall AdS-QCD model. *JHEP*, 12:113, 2022.
- [67] Weijian Liang, Xuanmin Cao, Hui Liu, and Danning Li. Pion quasiparticles in isospin medium from holography. *Phys. Rev. D*, 108(9):096019, 2023.
- [68] Niko Jokela, Matti Järvinen, and Jere Remes. Holographic QCD in the Veneziano limit and neutron stars. *JHEP*, 03:041, 2019.
- [69] Matti Järvinen. Holographic modeling of nuclear matter and neutron stars. *Eur. Phys. J. C*, 82(4):282, 2022.
- [70] Lin Zhang and Mei Huang. Holographic cold dense matter constrained by neutron stars. *Physical Review D: Particles and Fields*, 106(9):096028, 2022.
- [71] Kazem Bitaghsir Fadafan, Jesus Cruz Rojas, and Nick Evans. Holographic description of color superconductivity. *Phys. Rev. D*, 98(6):066010, 2018.
- [72] Kazem Bitaghsir Fadafan, Jesús Cruz Rojas, and Nick Evans. Deconfined, Massive Quark Phase at High Density and Compact Stars: A Holographic Study. *Phys. Rev. D*, 101(12):126005, 2020.
- [73] Kazem Bitaghsir Fadafan, Jesús Cruz Rojas, and Nick Evans. Holographic quark matter with colour superconductivity and a stiff equation of state for compact stars. *Phys. Rev. D*, 103(2):026012, 2021.
- [74] P. Colangelo, J. J. Sanz-Cillero, and F. Zuo. Holography, chiral Lagrangian and form factor relations. *JHEP*, 11:012, 2012.
- [75] Masayasu Harada, Yong-Liang Ma, and Shinya Matsuzaki. Chiral effective theories from holographic QCD with scalars. *Phys. Rev. D*, 89(11):115012, 2014.
- [76] Joshua Erlich, Emanuel Katz, Dam T. Son, and Mikhail A. Stephanov. QCD and a holographic

- model of hadrons. *Phys. Rev. Lett.*, 95:261602, 2005.
- [77] Leandro Da Rold and Alex Pomarol. The Scalar and pseudoscalar sector in a five-dimensional approach to chiral symmetry breaking. *JHEP*, 01:157, 2006.
  - [78] Andreas Karch, Emanuel Katz, Dam T. Son, and Mikhail A. Stephanov. Linear confinement and AdS/QCD. *Physical Review D: Particles and Fields*, 74(BUHEP-06-02, INT-PUB-06-04):015005, 2006.
  - [79] Kaddour Chelabi, Zhen Fang, Mei Huang, Danning Li, and Yue-Liang Wu. Realization of chiral symmetry breaking and restoration in holographic QCD. *Physical Review D: Particles and Fields*, 93(10):101901, 2016.
  - [80] Kaddour Chelabi, Zhen Fang, Mei Huang, Danning Li, and Yue-Liang Wu. Chiral phase transition in the soft-wall model of AdS/QCD. *JHEP*, 04:036, 2016.
  - [81] Zhen Fang, Yue-Liang Wu, and Lin Zhang. Chiral phase transition and meson spectrum in improved soft-wall AdS/QCD. *Physics Letters B*, 762:86–95, 2016.
  - [82] Yuki Fujimoto, Kenji Fukushima, Larry D. McLerran, and Michal Praszalowicz. Trace Anomaly as Signature of Conformality in Neutron Stars. *Phys. Rev. Lett.*, 129(25):252702, 2022.
  - [83] Eemeli Annala, Tyler Gorda, Aleksi Kurkela, Joonas Nättilä, and Aleksi Vuorinen. Evidence for quark-matter cores in massive neutron stars. *Nature Phys.*, 16(9):907–910, 2020.
  - [84] J. A. Wheeler. Geons. *Phys. Rev.*, 97:511–536, 1955.
  - [85] David J. Kaup. Klein-Gordon Geon. *Phys. Rev.*, 172:1331–1342, 1968.
  - [86] O. S. Stashko, O. V. Savchuk, L. M. Satarov, I. N. Mishustin, M. I. Gorenstein, and V. I. Zhdanov. Pion stars embedded in neutrino clouds. *Physical Review D: Particles and Fields*, 107(11):114025, 2023.